npj | flexible electronics

www.nature.com/npjflexelectron

ARTICLE OPEN

Check for updates

Imperceptive and reusable dermal surface EMG for lower extremity neuro-prosthetic control and clinical assessment

Jaeu Park[1], Jinwoong Jeong[1], Minseok Kang[1], Nagwade Pritish[1], Youngjun Cho[1], Jeongdae Ha[1], Junwoo Yea[1], Kyung-In Jang[1], Hyojin Kim[2], Jumin Hwang[2], Byungchae Kim[3], Sungjoon Min[3], Hoijun Kim[4], Soonchul Kwon[4], ChangSik John Pak[2], HyunSuk Peter Suh[2], Joon Pio Hong[2] and Sanghoon Lee[1]✉

Surface electromyography (sEMG) sensors play a critical role in diagnosing muscle conditions and enabling prosthetic device control, especially for lower extremity robotic legs. However, challenges arise when utilizing such sensors on residual limbs within a silicon liner worn by amputees, where dynamic pressure, narrow space, and perspiration can negatively affect sensor performance. Existing commercial sEMG sensors and newly developed sensors are unsuitable due to size and thickness, or susceptible to damage in this environment. In this paper, our sEMG sensors are tailored for amputees wearing sockets, prioritizing breathability, durability, and reliable recording performance. By employing porous PDMS and Silbione substrates, our design achieves exceptional permeability and adhesive properties. The serpentine electrode pattern and design are optimized to improve stretchability, durability, and effective contact area, resulting in a higher signal-to-noise ratio (SNR) than conventional electrodes. Notably, our proposed sensors wirelessly enable to control of a robotic leg for amputees, demonstrating its practical feasibility and expecting to drive forward neuro-prosthetic control in the clinical research field near future.

npj Flexible Electronics (2023)7:49 ; https://doi.org/10.1038/s41528-023-00282-z

INTRODUCTION

Flexible and stretchable electronic devices with excellent mechanical properties adaptable to the skin have tremendous advantages in healthcare applications, especially in the field of neuroprosthetics[1–4]. Surface electromyography (sEMG) sensors that record muscle signals on the skin are used as a clinical indicator to help with rehabilitation and treat diseases in a noninvasive manner[5,6]. In recent, researchers have been increasingly developing sEMG interfaces using soft materials and innovative designs. A notable illustration of such is the high-density sEMG (HDsEMG) electrode[7] introduced by Murphy et al. This electrode is 8 µm in thickness and offers a range of desirable qualities, including compatibility with skin, a hydrophilic surface, strong conductivity, minimal interfacial impedance, flexibility, and the ability to record across 16 channels. Driscoll et al. also utilized a modified fabrication approach to create a comparable sEMG interface utilizing MXene[8]. Their work goes beyond just recording signals, as evidenced by their successful use of the electrode to stimulate bio-potential signals in vivo experiments. Similarly, Yu et al. have made sEMG electrodes by utilizing a variety of nanomaterial inks[9]. The signal detection capabilities of their sensor are truly remarkable, especially when combined with the incorporation of a serpentine-structured electrode. This addition not only increases the design's elasticity but also improves its mechanical compliance. Zeng et al. have made sEMG electrodes in their use of hydrographic printing technology for fabrication, By integrating these electrodes into the skin, they are able to take advantage of its natural stretchability[10]. Huang et al. have made stretchable and flexible nanofibrous carbon film sensing electrodes[11]. This technology includes ingeniously interwoven textile-based sEMG sensors into clothing to minimize user awareness. The use of carbon as the conductive medium renders these interfaces chemically resistant, washable, and well-suited for skin contact. Microneedle EMG interfaces are another promising option, offering improved accuracy and easy attachment to the skin. Li et al. have shown polyimide-based microneedle array (MNA) electrodes' remarkable endurance, withstanding continuous usage among healthy subjects for 44 days[12]. Minimal penetration marks were observed upon detachment, dissipating within hours. These interfaces are vital, given the increasing need for extrinsic neural control of prosthetic devices using biosignals over the past decade to overcome the limitations of conventional autonomous-based prosthetic control[13–15].

Nonetheless, there are still no robust muscle interfaces for recording EMG signals from amputees, which makes the commercialization of bionic limbs controlled by biological signals difficult. In particular, the development of surgical techniques for amputation, such as agonist-antagonist myoneural interfaces (AMIs) and targeted muscle reinnervation (TMR), requires practical sEMG signals being used for advanced neuroprosthetic systems for amputees[16,17]. The main significant challenge is related to sEMG sensors for lower extremity amputees who wear a silicone liner that covers a residual limb and a socket that physically connects and fixes the prosthesis[18]. Typically, extremely dynamic pressure is applied to the socket during the gait cycle. Accordingly, close contact between the skin and the silicone liner is required to protect the residual limb from impact and fix the heavy prosthesis. Conventional sEMG sensors between a silicon liner and the skin cannot survive such harsh conditions[19,20]. To overcome this limitation, a customized sEMG sensor integrating electrodes and sockets was reported, but it is incompatible with other sockets, so it has low versability and requires high cost[21]. Additionally, more recently, Sub-Liner Interface for Prosthetics (SLIP) electrodes developed by Yeon et al. were manufactured

[1]Department of Robotics and Mechatronics Engineering, DGIST, Daegu 42899, Republic of Korea. [2]Department of Plastic and Reconstructive Surgery, Asan Medical Center, Seoul 05505, Republic of Korea. [3]Hugo Dynamics, HUGO, Hwaseong-si, Gyeonggi-do 18468, Republic of Korea. [4]Department of Smart Convergence, Kwangwoon University, Seoul 01897, Republic of Korea. ✉email: hoonw@dgist.ac.kr

using polyimide films as base substrates using gold as electrode materials[22]. This sEMG is about 80–100 µm thick and was developed using flexible printed circuit board (FPCB) manufacturing technology, so it has good reproducibility and versatility. They successfully demonstrated the human-machine interaction of SLIP electrodes by conducting clinical trials on people with lower limb amputations. However, the absence of surface adhesive layers requires medical tape and flexible but less elastic materials such as FPCBs have limitations that are vulnerable to mechanical perturbation and long-term use. And there's no way to deal with waste like sweat from the inside. This situation shows limitations in implementing advanced extrinsic neural prosthesis technology driven by amputees' intentions. Therefore, developing an sEMG sensor that can comfortably and stably record muscle signals for amputees in long-term use is urgently necessary.

The expected requirements of sEMG materials for amputees are (1) flexible and soft materials that have elasticity and flexibility similar to those of the skin for high-quality recording and sufficient for bearing the dynamic pressure during the gait cycle, maintaining the functionality, and (2) adhesive and breathable materials that allow attachment to the required targeted skin several times and evaporation of sweat and secretions from the amputee's skin, which are critical causes of degradation of the recording quality in long-term use. Furthermore, optimization of the electrode design to maximize the recording performance is required for amputees, who typically show lower muscle signals due to amputation than ordinary people. In this paper, we propose a medical band-like thin, stretchable, but imperceptive and reusable sEMG sensor for amputees with lower limb amputation who want to control lower extremity neuroprostheses. Our approach involves designing an sEMG device that enables recording of high-quality muscle signals while walking by stably and repeatably attaching to the skin surface with elasticity and flexibility (see Fig. 1a).

During the walking stage, some major muscles are differently activated depending on the phase, as shown in Fig. 1b[23]; thus, we demonstrate our multiple electrodes for each agonist and antagonist muscle to control the bionic limbs by identifying the amputee's muscular signals. To achieve our goals, we suggest a thin, stretchable, breathable, and reusable patch-type sEMG electrode (see Fig. 1a, c). The electrode pattern of the device is designed in a serpentine form to allow stable changes with the expansion and contraction of the deformed skin. The device consists of a silicon substrate layer and an electrode layer composed of polyimide (WPR-1021, JSR Corporation, Tokyo, Japan) as shown in Fig. 1c. The electrode layer is fabricated by a typical microfabrication process, and a gold electrode is used as a conducting electrode. For the substrate layer, polydimethylsiloxane (Sylgard® 184 PDMS, Dow Corning, Midland, Texas) and Silbione (Silbione® 4717, Elkem Silicones, Oslo, Kingdom of Norway) are used. We also aim to address the problem of sweat-like secretions from the skin by modifying the molecular structure of the substrate of the device to facilitate the release of secretions and using chemically safe and long-life metal materials as electrodes. Additionally, by making the electrode thin and soft similar to the skin, we minimize the feeling of foreign substances to almost imperceptive when attached to the inside of the socket and the liner worn to fix the skin. In summary, breathability and porosity are attained with biocompatible PDMS, and Silbione, which is an adhesive silicone material, facilitates attachment to the skin and transfer of the electrode layer to the substrate layer (Supplementary Fig. 1). Moreover, Silbione exhibits inherent permeability and exceptional adhesion properties compared to another polymer substrate products[24,25]. We demonstrate that an amputee successfully tested the walking assistance through robotic control based on EMG signals, indicating that this sEMG sensor can be applied to the rehabilitation and treatment areas of amputees and can be used in various artificial prostheses and robot control.

RESULTS

Characteristics of the substrates

The fabricated imperceptive sEMG sensor has a total thickness of 170 µm, consisting of 38 µm for the electrode layer and 132 µm for the substrate layer, as illustrated in Fig. 1c. Porous polydimethylsiloxane (P-PDMS) was used as the substrate material. Figure 1d shows the surface change of P-PDMS according to the change in the citric acid concentration. Crystallization and removal of the citric acid mixed with PDMS result in the formation of micro sized holes within the PDMS, increasing the breathability[26]. The detailed fabrication is described in Supplementary Fig. 2. As shown in Fig. 1e, the thickness of P-PDMS affects the water vapor transmission rate (WVTR). The result showed that P-PDMS with a thickness of 50 µm achieved a WVTR of 475 g m^{-2} day^{-1}. For Silbione, Cho et al. reported a WVTR of 2755 g m^{-2} day^{-1} for Silbione® 4717 with a thickness of 0.5 mm[24]. To investigate a WVTR of the final substrate, we conducted a WVTR test on a substrate layer coated with 80 µm of Silbione on a P-PDMS with a thickness of 50 µm. The WVTR result of the substrate layer is 257 g m^{-2} day^{-1} ($n = 2$) indicating a more favorable attachment environment than the typically emitted by humans per day of 204 g m^{-2} day^{-1} [27–29]. The Young's modulus of the substrate layer was investigated. Figure 1f shows the result of the stress-strain curve for the substrate layer. The equipment was clamped to an end of the 5 cm square substrate and stretched at a 20 mm min^{-1} speed. The Young's modulus of the substrate layer is 145.38 kPa, which is very similar to the Young's modulus of skin in the literature, and it can withstand strain up to 35%. These characteristics of the substrate layer enable close contact between the skin and the interface even under deformation conditions, thus facilitating the development of imperceptive sEMG technology.

Design and mechanical test

Amputees exhibit muscle reduction in the amputation region, leading to distinct variation in limb contour in comparison to individuals without amputations. Consequently, sensors are required for a substantial degree of elasticity, flexibility, and higher recording performance to accommodate these conditions[3,30]. To determine the optimal electrode pattern, we referred to previous studies[4]. Chandra et al. found that theta (θ) is most elastic at 45° and the width (W) improves elasticity proportionally. Thus, we set theta to 45° and scaled the pattern to increase electrode width and area for better signal quality and elasticity. Figure 2a shows the design of an island-type electrode with a 90° crossing of serpentine lines, enabling simultaneous stretching along the *x*- and *y*-axes. By adjusting pattern density, we developed small electrodes with high density, large electrodes with low density, and medium sized electrodes. Numerous studies have embraced a meandering structural approach in sEMG designs to enhance their adaptability to mechanical deformation[3,31–33]. However, our proposed design additionally features a two-electrode configuration as the sensing electrode, following the guideline of SENIAM's recommendations[34]. To significantly increase the active surface of the electrode, we increased both the width and height, and incorporated an island structure pattern for effectively mitigating impedance reduction. This approach not only maintains the overall surface area but also provides stretchability, optimizing the performance of the sensor.

COMSOL simulations were conducted to investigate the relationship between stress and strain for the electrodes with the three different densities (see Fig. 2b). The simulation results indicated that all three patterns can be stably attached to the skin without cracking the metal and can be stretched, with a value of

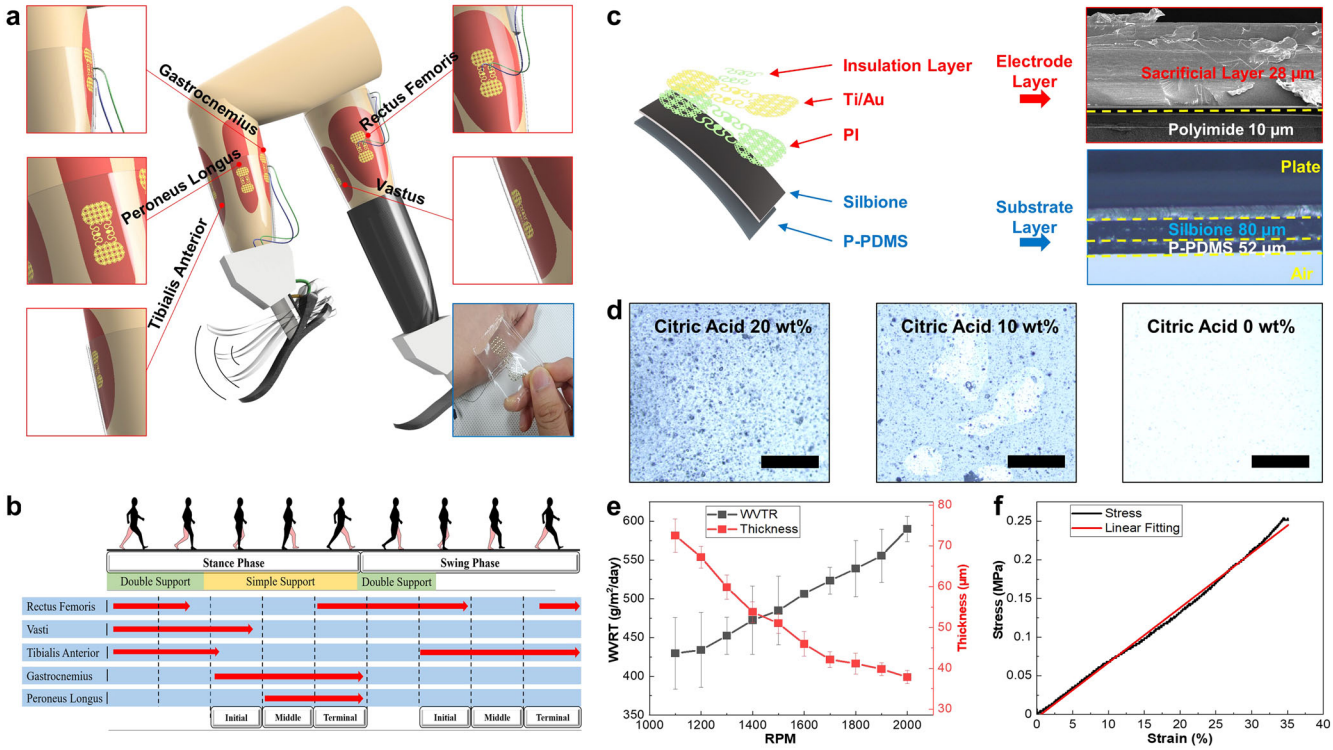

Fig. 1 Schematic illustration of the flexible and stretchable sEMG sensors designed for amputees. a sEMG sensor attached to different types of muscles in the legs. The red boxes show graphically implemented images, and the blue box presents a picture of the fabricated sEMG sensor. **b** Muscle parts are activated at different times depending on the gait phase. **c** Specific description of the electrode layer and base layer of the sEMG sensor. Cross-sectional photographs of the electrode layer and substrate layer were obtained by scanning electron microscopy (SEM) and a microscope. The yellow dotted line indicates the boundary of each side. **d** Microscopically photographed surfaces of P-PDMS according to the citric acid concentration (scale bar, 1 mm). **e** Graph for the breathability test of P-PDMS (**e**, $n = 20$ samples for WVTR, and $n = 3$ samples for thickness, data presented as mean ± s.d.). **f** Graph of the stress-strain curve of the substrate layer. The calculated tensile stress is 253.85 kPa, and Young's modulus is 145.38 kPa.

less than 120 MPa up to 30% elongation. For the small high-density electrode with the smallest width, 120 MPa occurs in the pattern when it is elongated by 146%. For the medium-density electrode, 120 MPa occurs at 90% elongation, and for the large low-density electrode, it occurs at 39% elongation. Considering the yield stress of Au[35] and the deformation degree of the skin[36], the results show that the electrodes with all three densities can withstand the pressure applied between the socket and the skin. The design with the greatest stretching force for the three patterns is the small high-density pattern, which is due to the thinnest line width of the metal pattern. Additional simulations were carried out to assess electrode stability against skin deformations such as contractions and twisting, but tensile deformation was found to be the most significant (Supplementary Fig. 3).

Figure 2c shows the three patterns with different densities in the form of electrodes. For patch-type electrodes with a size of less than 2 cm, the area exposed to the outside differs depending on the pattern density. The area was measured for each density pattern, resulting in values of 68.33 mm^2 for the large electrode, 63.88 mm^2 for the medium electrode, and 60.30 mm^2 for the small electrode. This can be converted into the filling factor, which is the ratio of the exposed area to the ellipse area (the head part), and the large pattern electrode has the highest value at 53%, followed by the medium electrode at 50% and the small electrode at 47%. The impedance of the large pattern is expected to be lower, as the contact impedance at the skin-electrode interface is related to the electrode-skin contact area.

Figure 2d shows the resistance and strain results for the electrodes obtained using a bending machine. The elongation speed was 0.1 m s^{-1}, with extension up to 80%, and the change in the resistance for the *x*- and *y*-axes was observed by connecting wires to the black dots in all three density patterns. In all the patterns, the change in the resistance in the *x*-axis direction was larger than that in the *y*-axis direction, which might be due to the body structure of a straight line in the *x*-axis direction from the head part (patterned electrode) leading to the connector. For *y*-axis tension, all three density pattern electrodes showed less than a 10% change in the resistance up to 60% elongation. Contrary to the simulation results, the large low-density pattern had the lowest resistance change rate for the *x*-axis, and then, the stability decreased in the order of small and medium. The overall resistance changes were stable within 30% strain, indicating that the fabricated sensor could be used for muscle signal recording.

Performance comparison by pattern density

Before moving to muscle recordings from amputees, we compared the performance of the EMG sensors with different pattern densities for a normal person's muscle, especially for large deformation. The EMG sensors were attached to the biceps, and commercial electrodes (Com) were attached to the elbows as ground, as shown in Fig. 3a. Muscle contraction and relaxation were repeated at a cycle of ~10 s, and the muscle signals in the biceps were measured (see Fig. 3b). The EMG signal was measured by connecting an Intan Board system and a differential amplifier. The detailed recording setup is described in the Methods section. The signal-to-noise ratio (SNR) was calculated to evaluate the performance of the sensors. The results show that the large pattern low-density electrode has the best signal recording ability, with an SNR of 24.68 dB, followed by the medium and small

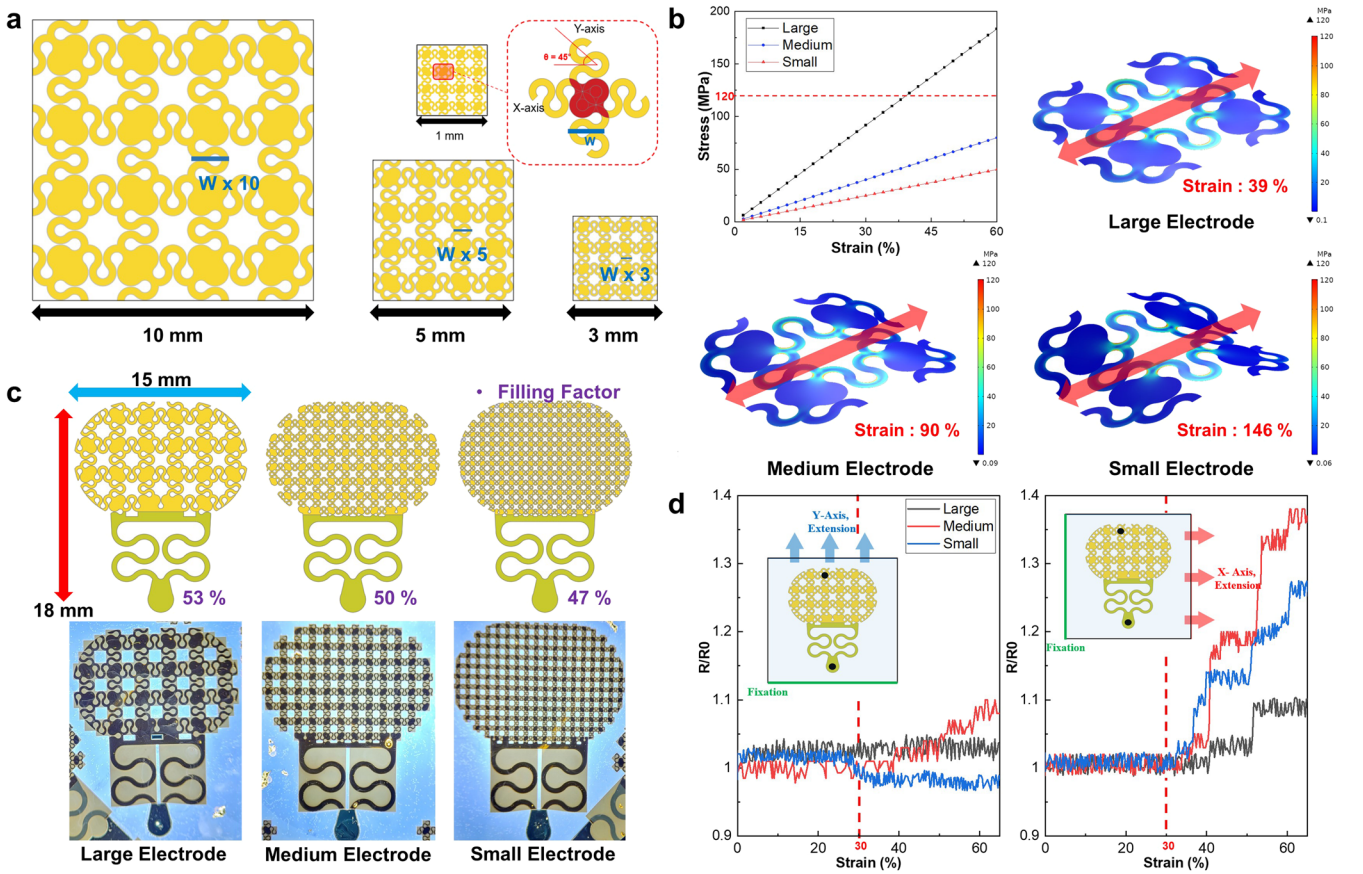

Fig. 2 Design and mechanical characteristics of the proposed sEMG electrodes. a Design of unit patterns forming the electrodes. The red dotted box shows the smallest part of the pattern. **b** Stress-strain curve graph of patterns calculated based on the numerical analysis simulation tool. The red arrow points in the direction of tension. **c** Description of single electrode designs with three density patterns**. d** Graph measuring the changes in the resistance according to the tensile strain of the device. Both sides of the substrate layer were fixed with a clamp of the equipment, and the substrate was stretched in the direction of one clamp. The resistance meter was connected to the black dot to observe the amount of resistance change.

pattern electrodes, with SNRs of 23.01 dB and 20.06 dB, respectively (see Fig. 3c). The low-density large pattern outperformed commercial electrodes in recording signal quality. And the medium-density pattern also showed similar SNR values to commercial electrodes but with better resistance to deformation compared to other patterns. Considering amputee's various contours, these both patterns were developed with careful consideration for amputees. we fabricated the large pattern electrode into a pair of new sensing electrodes (NSE) and the medium pattern electrode into a pair of old sensing electrodes (OSE). Also, NSE has more flexible design in connection part between the body and the pad. According to the electrode geometry recommended by SENIAM, the distance between a pair of electrodes (center to center) should be ~2 cm, and the size of the electrode should be ~1.5 cm (Supplementary Fig. 4)[34]. NSE included the improvement of changing the straight-line body structure to a serpentine structure to reduce the mismatch effect experienced above. The sensitivity of the EMG signals was measured with NSE as the sensing electrode and the large-pattern electrode as the ground electrode. To measure tensile force, we used a universal testing machine with a 1 kg steel ball attached. Participants were directed to extend their arms and relax their biceps while gripping the ball. We attached the proposed sEMG sensor to the bicep area to capture muscle signals in real time. The experiment involved participants performing four repetitions of bicep contractions followed by relaxation, each lasting 10 s (Sensitivity calculations are shown in the "Method"). Figure 3d provided results obtained from these exercises. The sensitivity calculated from the muscle signals obtained with NSE and LG was 5.17 $\mu V\,N^{-1}$. Under the same conditions, the calculated sensitivity for the commercial electrodes was a value of 4.04 $\mu V\,N^{-1}$ (Supplementary Fig. 5). The results of the experiment indicate that the low-density large-pattern EMG sensor has a higher sensitivity in detecting muscle signal variations compared to commercial electrodes. This finding highlights the great potential of the proposed sensor to be the ideal choice for driving robotic systems.

Assessment of the proposed sEMG sensor

To evaluate the performance of the sensors in lower limbs, we performed a comparative assessment using both NSE and OSE configurations on various body segments. Our systematic analysis aimed to assess the usability and performance of each configuration. To target the rectus femoris (RF), gastrocnemius (GC), and tibial anterior (TA) muscles of the lower leg, NSE, OSE, and Com were used as sensing electrodes, and LG and Com were used as ground electrodes for the knee, as shown in Fig. 4a. Before attaching the electrode, the leg hair was shaved, and the surface of the skin was cleaned using tape. The subject then repeated muscle contraction and relaxation for a certain period, and the muscle signals were recorded (see Fig. 4b). The signal processing procedure was applied to the recorded signals, and the SNR was calculated (see Fig. 4c). The highest SNR was obtained when NSE was used as the sensing electrode and LG as the ground electrode, which outperformed the SNR from commercial

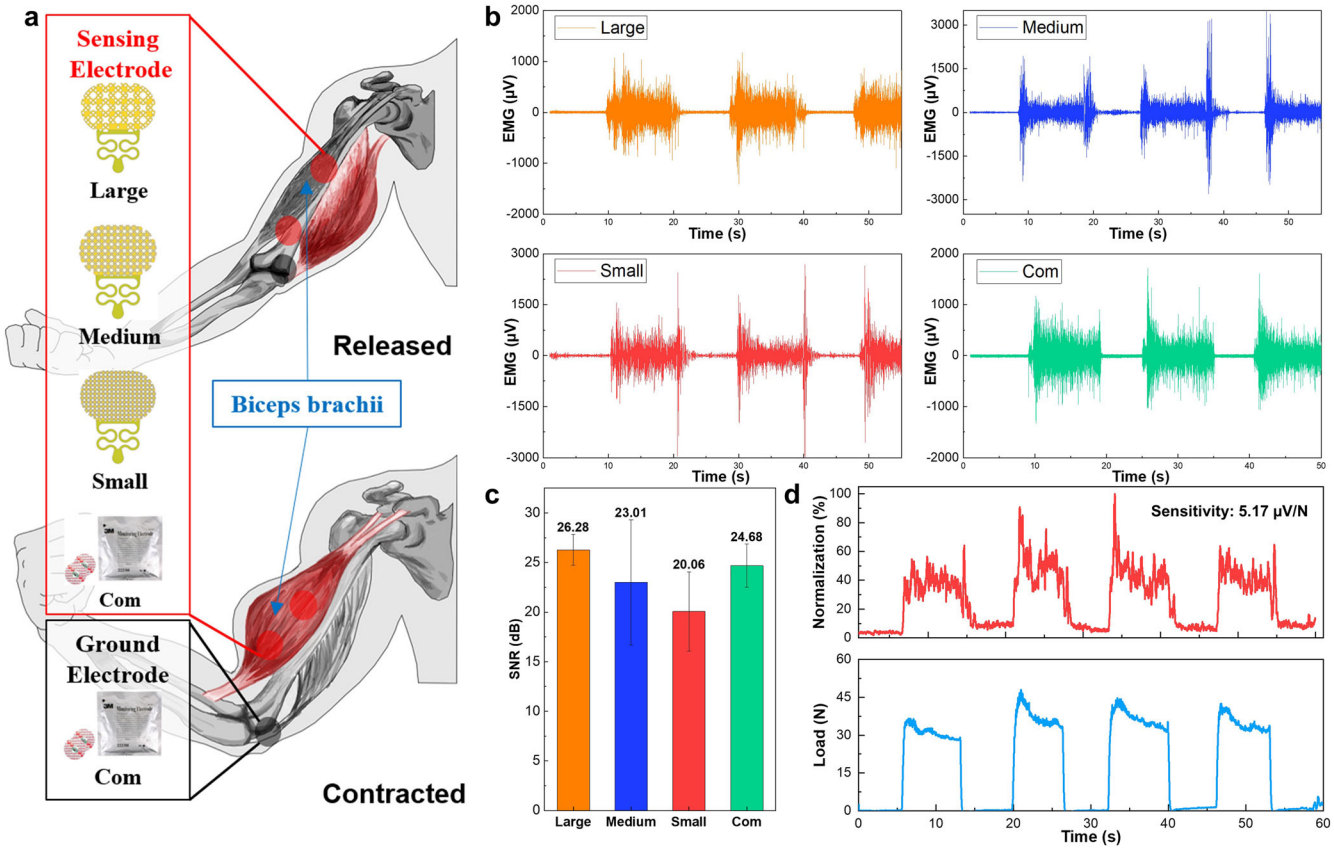

Fig. 3 SNR comparison by pattern density for biceps. a Commercial electrodes and EMG sensors of various pattern densities were attached to the subject's biceps. The red box represents the electrodes used as sensing electrodes, and the black box represents the ground electrode. The subject repeated muscle contraction and relaxation for a certain period. **b** Muscle signals measured from the biceps. The legend represents what kind of electrodes were used. **c** SNR calculated from muscle signals measured from each electrode pair (**c**, $n = 3$ trials, data presented as mean ± s.d.). **d** Sensitivity test graph measured using NSE as the sensing electrode and LG as the ground electrode.

electrodes. Furthermore, the time domain analysis of data from commercial Ag/AgCl electrodes and NSE electrodes aimed to quantify the signals' similarity. A calculation of Pearson correlation was performed using the data collected from commercial electrodes as a benchmark to evaluate the Interchangeability of these electrodes for prosthetic control applications[37]. The Pearson correlation coefficient ranges from +1 to −1, where +1 indicates perfect positive linear correlation, 0 indicates no linear correlation, and −1 indicates perfect negative linear correlation. As shown in Fig. 4d, NSE comprised of LG and Com both provide reliable indicators of a linear relationship. A Pearson correlation coefficient of 0.9254 is achieved when the NSE electrode is used as the sensing electrode and paired with the LG electrode as the ground electrode. Similarly, a Pearson correlation coefficient of 0.8940 is achieved when the NSE electrode is the sensing electrode with commercial as the ground electrode. It likely seemed that the same type of electrode pairs (dry-dry) showed better performance than different type pairs (dry-wet) for the recording. But it's clear that both types provide reliable indicators of a linear relationship, regardless of signal amplitude. This supports the use of either type for prosthetic control. Upon evaluating the ground electrode options, we found that the LG electrode yielded a slightly higher Pearson coefficient compared to the Com electrode and showed the highest SNR among three patterns. Therefore, we concluded that the LG electrode would be the optimal choice for our experiment.

To address the selectivity of recording muscle activity during ankle movement, muscle signals of the GC and TA muscles were simultaneously measured by the electrodes during both dorsiflexion and plantar flexion (see Fig. 4e). The electrode configuration refers to the use of NSE or OSE as the sensing electrode and LG as the ground electrode or to the use of Com as the sensing electrode and Com as the ground electrode. Figure 4f shows the recorded signals, where the red line represents TA muscle signals and the blue line represents GC muscle signals (the red and blue boxes indicate dorsiflexion and plantar flexion, respectively). Figure 4g, h shows the SNR results from the three electrode configurations during plantar flexion and dorsiflexion, respectively. When the agonist muscle GC was activated during plantar flexion, the Com-Com configuration showed the highest SNR of 37.33 dB, while those in the NSE-LG and OSE-LG configurations were 33.45 dB and 26.16 dB, respectively. At the same time, the SNRs from the antagonist muscle TA showed a similar tendency during plantar flexion. Interestingly, the ratio calculated as the agonist/antagonist muscle ratio showed the lowest value of 1.46 for the Com-Com pair, while the ratio for the OSE-LG pair showed the highest value of 2.59 (1.71 for the NSE-LG pair). This result might be because the higher impedance ignores signals, including noise coming from surroundings, other than the target muscle signal, ironically enhancing the selectivity ratio. From the point of view of robot operation, this higher selectivity ratio is crucial for clearly distinguishing which muscles are active. However, direct comparison is limited in that Com as a wet electrode makes defining the effective contact area with the skin difficult compared with the dry-type OSE and NSE. The metal area of Com is smaller than that of our electrodes, but the gel (Ag/AgCl) area is larger than that of ours. Additionally, the elliptical elongated electrode is different from the circular electrode of

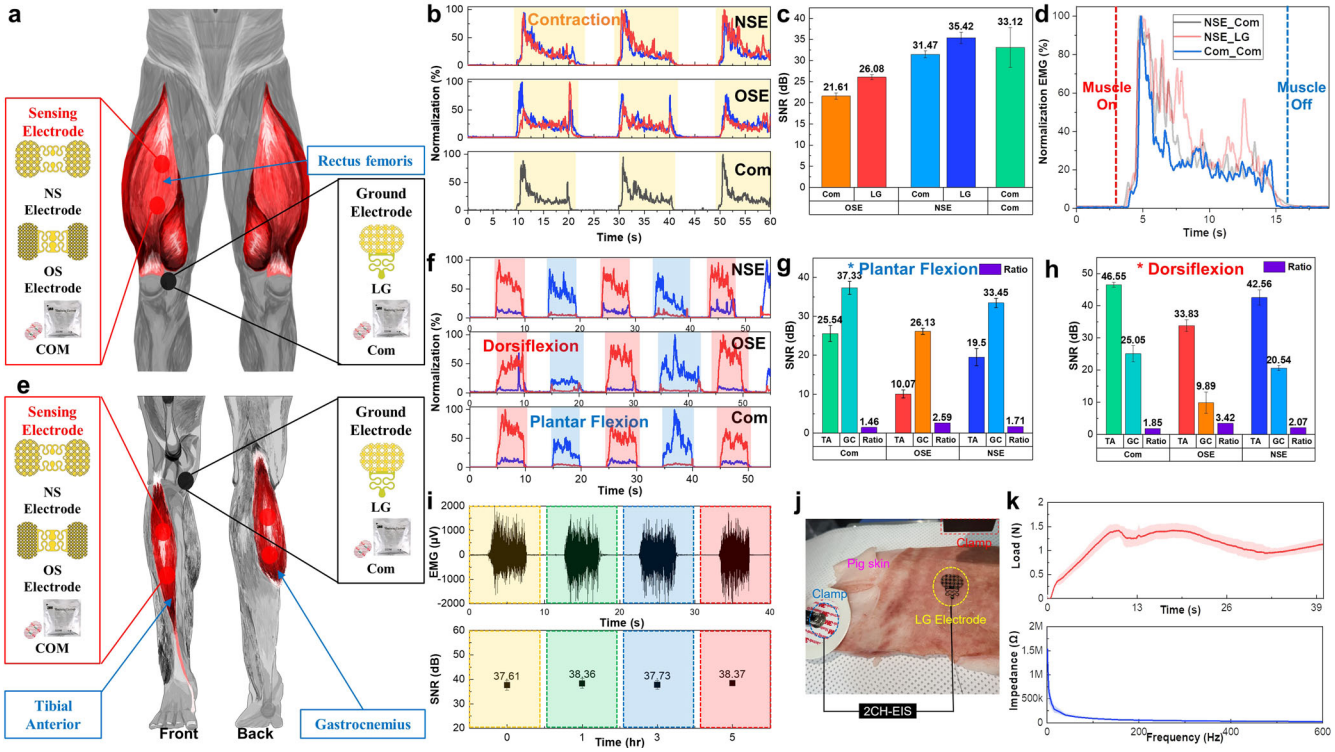

Fig. 4 Comparison of OSE and NSE for leg muscle. a Analysis of the signal acquisition ability using NSE, OSE, and Com as sensing electrodes for RF muscles and LG and Com as ground electrodes for knees. **b** Signals obtained from the RF muscle. The red signal is when LG is used as the ground electrode, and the blue signal is when Com is used as the ground electrode. When only Com was used, the signal is shown as a black signal. **c** SNR calculated from the RF muscle signals measured with each electrode pair. The bottom row represents the type of sensing electrode, and the top row represents the type of ground electrode (**c**, $n = 3$ trials, each electrode, data presented as mean ± s.d.). **d** Comparative analysis of muscle-on and muscle-off muscle signals. **e** Selective signal recording ability test for the TA muscle and GC muscles. Measurements were made with the NSE and LG configuration, OSE and LG configuration, and Com configuration. **f** Signals obtained from the TA and GC muscles. The red and blue signals were obtained from sensors attached to the TA and GC muscles, respectively. The red box represents the dorsiflexion section, and the blue box represents the plantar flexion section. **g**, **h** SNR calculated from the TA and GC muscle signals measured with each electrode pair (**g**, **h**, $n = 3$, data presented as mean ± s.d.). **i** Long-term use evaluation for the NSE (**i**, $n = 3$ trials, data presented as mean ± s.d.). **j** Picture of attaching and detaching the proposed sEMG sensor onto and from pig skin. **k** Force and impedance measured after ten consecutive attachment and detachment cycles.

Com. Even though the OSE-LG configuration showed the highest selectivity ratio, we prepared the NSE-LG configuration for clinical trials for amputees since a high SNR performance should also be considered due to degenerated muscles of amputees. This configuration showed a higher selectivity than Com and a higher SNR than OSE.

Prior to initiating clinical trials, we performed a comprehensive assessment of the long-term electrode performance on the TA muscle for a duration of 5 h while wearing a silicon liner. Figure 4i shows the results of the recorded signals and the SNR, indicating that the NSE-LG pair maintains its function for the entire duration of the test, despite the actual secretion of sweat under the silicon liner, which is identical to the product used by amputees. Furthermore, in Fig. 4j, we test the changes in the adhesion and impedance of the device upon repeated attachment. Given the remarkable similarity in terms of mechanical and biochemical properties, pig skin was chosen as a viable substitute for human skin in adhesion tests[38]. To evaluate the repeat and reuse performance of surface electromyography sensor pads, we designed an experiment based on a previous study[39]. To achieve our objectives, we attached an LG electrode and a commercial electrode to pig skin, followed by connecting the working and counter electrodes of the Electrochemical Impedance Spectroscopy (EIS) system. We fixed one side by using a clamp and peeling it off at 90°, repeating the process 10 times. Figure 4k displays the results, with the mean value represented by a solid line and the shaded region denoting the standard deviation range. Despite the repeated use of the device, the experiment yielded promising results, with no significant decrease observed in terms of adhesion or impedance, thereby demonstrating the suitability of the NSE-LG pair for long-term usage inside a silicon liner. This remarkable feature underscores its suitability for use in skin electronic devices, for which consistent and reliable adhesion is crucial, especially in environments characterized by increased moisture and perspiration. And the resistance changes in NSE according to the tensile strain were measured. Even when stretched to 50%, the change in the resistance did not reach 10%, and in the durability, test involving two-axis repeated stretching, the resistance change was less than 2% in the experiment, in which 30% stretching was repeated 600 times (Supplementary Fig. 6).

Assessment of the sEMG sensor in static condition for lower limb amputees

To evaluate the performance of the NSE-LG pair for use by lower limb amputees, the TA and GC muscle signals of a below-the-knee amputee were simultaneously measured using a wired system, as shown in Fig. 5a and Supplementary Fig. 7. The subject was a 30-year-old male with a history of amputation 8 years ago. The patient was unshaven, and after lightly wiping the epidermis of the target muscle with a cloth, the sEMG sensors were attached. The patient was requested to perform dorsiflexion and plantar flexion, and the recorded signals are shown in Fig. 5b. The SNRs of

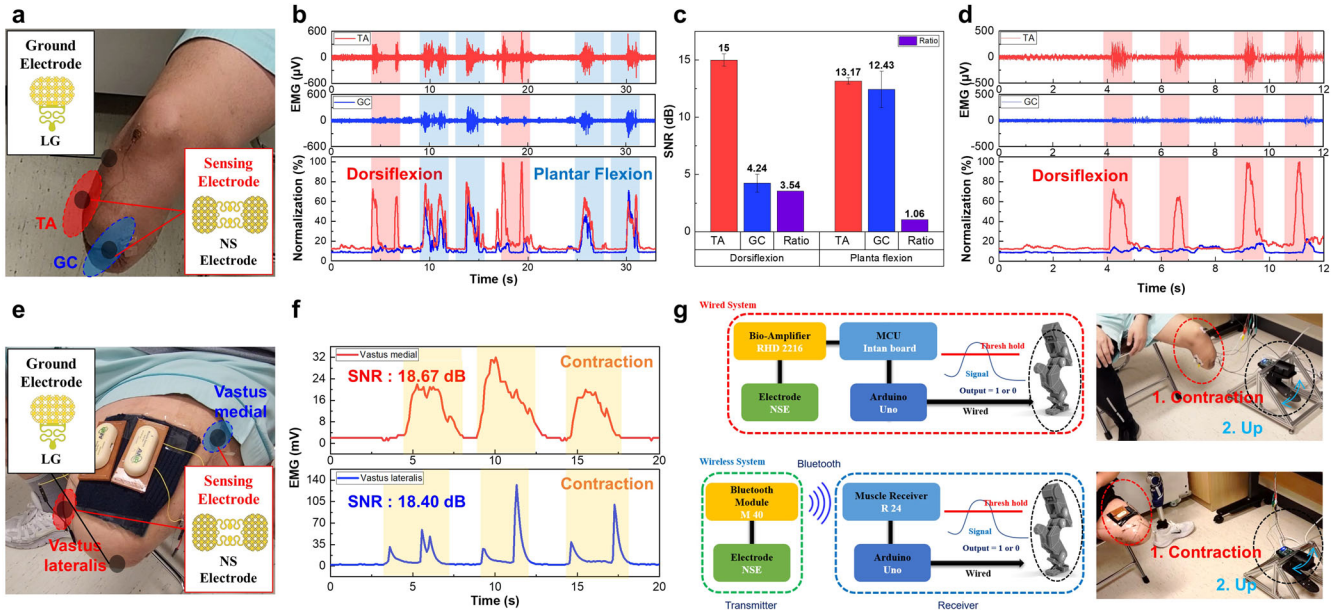

Fig. 5 Clinical trial of leg amputees. a Attachment of the proposed sEMG to the amputee's TA and GC muscles. The red box represents the electrodes used as sensing electrodes, and the black box represents the ground electrode. The subject repeated muscle contraction and relaxation for a certain period. **b** Muscle signals measured from the patient. The red and blue signals were obtained from electrodes attached to the TA and GC muscles, respectively. The top is the raw EMG signal, and the bottom is the normalized EMG signal. **c** SNR calculated from muscle signals measured from the dorsiflexion and the plantar flexion, respectively (**c**, $n = 3$ trials, each electrode, data presented as mean ± s.d.). **d** Muscle signal for dorsiflexion to drive the robot. **e** Demonstration of the wireless EMG signal acquisition system for the amputee's VM and VL muscles. **f** Wireless recorded EMG signals measured from the VL and VM muscles. **g** Setting method and photograph of wired and wireless systems for robot operation.

the signals were calculated, as shown in Fig. 5c. The results indicated that the SNRs were lower in the amputee than in nonamputees due to the lower degree of muscle activation. However, the ratio result from dorsiflexion was 3.54, which is an excellent result compared with the previous result. The ratio result from plantar flexion was 1.06, which is lower, and the TA and GC muscle signals could not be distinguished. This could be attributed to the limited activation of muscles in amputees even with the correct intention compared with nonamputees[40–42]. Notably, identifying the location of agonist and antagonist muscles is difficult, even with the help of a clinical assistant, due to the different surgical modalities of each amputee patient. Additionally, the degree of muscle activation individually varies depending on the amputee's lifestyle and the period after amputation[43].

To operate a robotic leg based on the EMG signal being recorded, only dorsiflexion, which showed an excellent ratio result, was requested for the patients. Figure 5d shows the muscle signal being recorded, and it was used to control the robotic leg. We set an appropriate threshold value based on the amplitude of muscle signals obtained in previous experiments. When the raw muscle signal from the TA muscle crossed the threshold, it was output to the robotic leg for operation. This threshold was adjusted to properly operate the robotic leg during the experiment. The calculated SNR was 18.97 dB, and the robot was successfully driven based on this experimental setup. It can be observed that the robotic leg also maintains dorsiflexion while contracting muscles (Supplementary Movie 1).

Furthermore, the vastus lateralis (VL) and vastus medial (VM) muscle signals of an above-the-knee amputee were simultaneously measured using a wireless system, as shown in Fig. 5e and Supplementary Fig. 8. The subject was a 49-year-old male with a history of amputation 25 years ago. The patient was unshaven, and after lightly wiping the epidermis of the target muscle with a cloth, the sEMG sensors were attached. The patient was requested to apply force to each muscle, and the recorded signals are shown in Fig. 5f. The EMG signal was recorded via the commercial wireless recording system, so the rectified and smoothed signals were recorded through its software. The calculated SNRs of the VM and VL muscles were 18.67 and 18.40 dB, respectively, which are similar to those measured by a wired system. Due to the limitations of the system, muscle signals in both areas could not be measured at the same time, so the experiments were conducted separately. Since clear signals were recorded, the robotic leg could be controlled by the biosignals, and simple control was successfully performed (Supplementary Movie 2 operated by the VM muscle signal).

The robotic leg was operated with both wired and wireless systems, and Fig. 5g shows each schematic. In the wired system, we recorded the signal from the fabricated electrode and output the signal to the output pin of an Intan Board when the signal was above the threshold through the Intan RHX software. In the case of the wireless system, the signal was transmitted through Bluetooth communication between the M40 Muscle Sense wireless module and the R24 antenna. The AC signal outputs were converted from the raw EMG data in an Arduino IDE for smooth robot control.

Assessment of the sEMG sensor in dynamic condition for lower limb amputees

To evaluate the sEMG sensors in dynamic conditions, we conducted an experiment on a 39-year-old man who underwent amputation and regenerative peripheral nerve interface (RPNI) surgery 3 years prior. The NSE was attached as a sensing electrode to the patient's right leg GC and TA muscles, respectively, while the LG was attached as a ground electrode to the knee (see Fig. 6a, 1–2). After that, he wore a silicone liner and connected the lower prosthesis (Fig. 6a, 3). A wireless system module consisting of a Raspberry Pi and an Intan Arduino Shield, as shown in Supplementary Fig. 9, was attached to the socket to record muscle signals during ambulation (see Fig. 6a, 4).

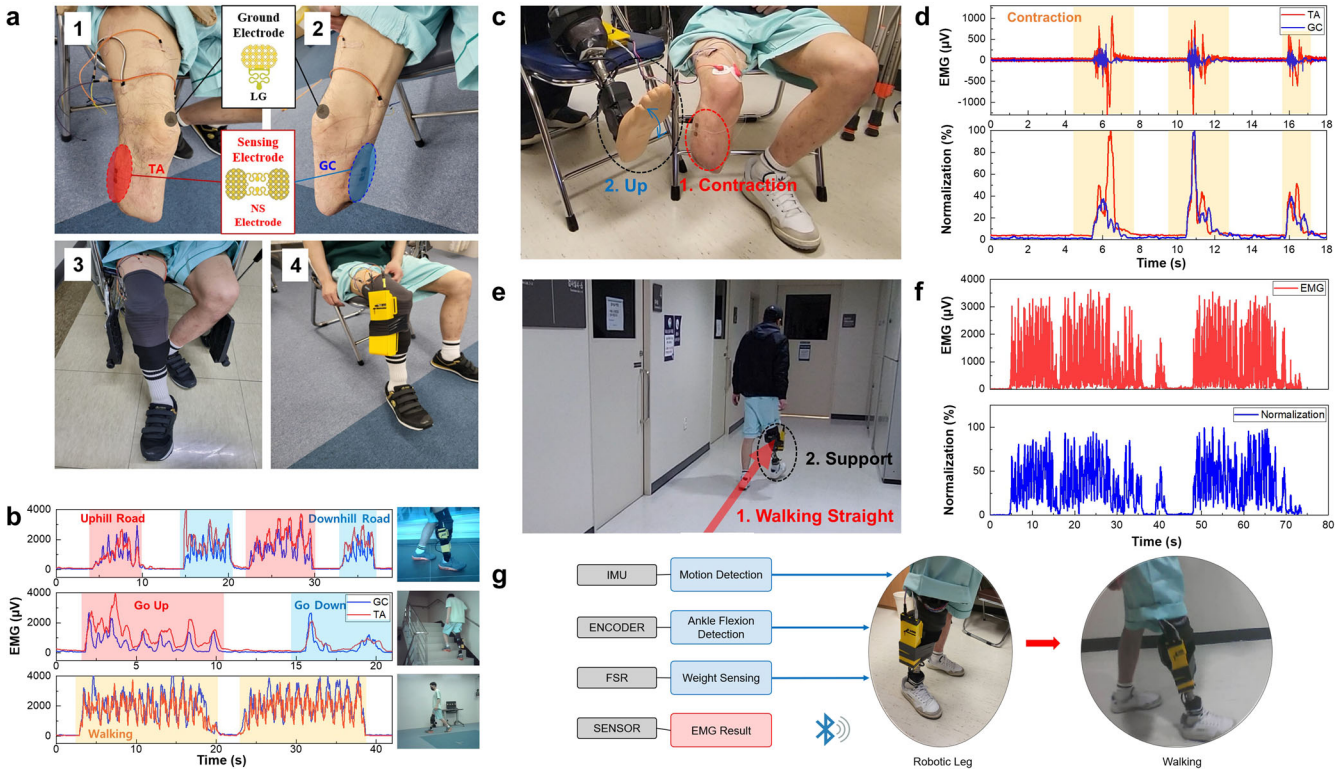

Fig. 6 Observation of an RPNI amputee using a wireless electromyography system in the dynamic case. a Photograph of the suggested sEMG system for patients with RPNI lower leg amputation. We attached the proposed electrode to the TA and GC muscles of the amputee, who wore a liner and a robotic leg, and finally installed the wireless system. **b** Muscle signals measured in dynamic situations. The patient walked on flat land, uphill, and stairs, and signals were accordingly obtained. **c**, **d** EMG signals obtained from the TA and GC muscles. The threshold of the TA signal and GC signal is selected and used to drive the robot. **e**, **f** EMG signals obtained from the GC muscle. The system helps with walking by utilizing muscle signals that exceed the threshold while walking with IMU and FSR sensors built into the robotic leg. **g** Protocol of the walking support system. The robotic leg detects mechanical motion through IMU, ENCODER, and FSR sensors and biological signals through the proposed sEMG sensor.

Although the patient was requested to perform dorsiflexion and plantar flexion, he could not activate the TA and GC muscles separately, unlike the previous subject, who underwent amputation 8 years prior. Again, muscle signals in amputees are influenced by a variety of variables, such as surgical methods, the period after amputation, the extent of amputation, the state of remaining nerves, and lifestyle (whether amputees live an active life with exercise and so on)[43]. Nevertheless, the patient attempted to walk in various environments (flat land, uphill, and stairs), and we stably recorded the signals, as shown in Fig. 6b. According to the different ambulation conditions, the muscle activations showed clearly different patterns. Furthermore, we recorded the signals while the patient walked on a treadmill, as shown in Supplementary Movie 3.

On another day, we conducted a further experiment with the same patient. We requested that the subject perform dorsiflexion of the leg as much as possible and recorded the muscle signals (Fig. 6c). As shown in Fig. 6d, the patient activated both the TA and GC muscles due to being incapable of contracting each muscle individually. The calculated ratio was 1.31, which is not a good value. Additionally, the recorded signal was used for robotic leg control (Supplementary Movie 4).

The wireless module, consisting of a Raspberry Pi system, was able to record and observe two muscle signals at the same time through WiFi and was connected to the robotic leg by Bluetooth to enable robot control. As before, the patient's signal was observed, and an appropriate threshold was selected to allow the robotic leg to respond to signals beyond that threshold. Following the success of simple robot control during sitting, we applied the muscle signals to robot control during ambulation (see Fig. 6e). Figure 6f shows the muscle signal recorded when the patient walked with the robotic leg. According to the control protocol, signals are received by the robotic leg through Bluetooth and interact with built-in sensors to help the patient successfully walk (Supplementary Movie 5). A more specific system configuration is shown in Fig. 6g. IMU, ENCODER and FSR sensors were used to detect patient movement, center of gravity, and ankle movement. In addition, if the self-walking algorithm conditions are met, then the activation trigger is provoked by control commands received from the wireless EMG system. One biosignals was sufficient to help with walking assistance, so we designed the experiment to observe GC muscle signals obtained from wireless EMG systems, select arbitrary threshold values, and transmit control commands to robotic legs via Bluetooth communication.

DISCUSSION

This study demonstrated a flexible and stretchable sEMG interface with a serpentine design that is compatible with human skin. The use of materials with stretchability and flexibility enabled the interface to withstand a 30% tensile force, as indicated by the simulation, and to demonstrate excellent mechanical characteristics, as measured by the resistance change. Furthermore, the proposed sEMG interface provided stable signal acquisition for long-term use. We evaluated the signal acquisition performance in both static and dynamic muscle states. For instance, for the RF muscle, the recorded signals showed an excellent SNR of 35.42 dB, and better behavioral distinction was possible with the clear selectivity ratio in TA and GC muscle signal measurements compared to commercial electrodes. Additionally, we conducted

tests of the proposed sEMG in both static and dynamic conditions for amputee patients and successfully demonstrated simple robotic leg control and walking support. An important feature to highlight is the exceptional adhesive properties of Silbione, particularly its ability to maintain strong adhesion even on sweaty skin[39,44,45]. By integrating Silbione and P-PDMS, the device was repeatedly attached and detached from the patient during the experiment over several hours, consistently capturing muscle signals with exceptional stability and reliability. The goal of the next step is to apply the muscle signals of amputee patients to their daily lives by enabling precise and accurate control through pattern analysis using artificial intelligence (AI).

To realize next-generation advanced prostheses, collaboration across various fields, including neurology, mechanics, and material science, is essential[46,47]. The absence of sensory information and motor nerves in amputated limbs poses functional and cognitive disadvantage when using advanced prostheses[48–50]. To address this challenge, it is imperative to study the benefits of supplementing sensory information and understand the underlying mechanisms[51]. The custom-designed advanced EMG sensor for amputee patients is a valuable tool for diagnosing and treating muscle conditions in clinical evaluations and rehabilitation, thus assisting patients in walking through robot control. The NSE device consists of a combination of a porous PDMS structure, a substrate layer coated with a biocompatible silicone adhesive, and an electrode layer with good tensile durability and electrical properties. It offers excellent breathability and skin compatibility, ensuring stable signal acquisition over extended periods within the socket for amputees with various contours. Consequently, by acquiring and analyzing physiological signals, healthcare professionals can gather and utilize pathological data for diagnosing and treating various diseases. Furthermore, this approach can be employed in an advanced neuroprostheses that aid in walking based on the patient's intentions. The advanced EMG sensor, adaptable for placement inside the socket of any type of prosthetic type at any amputation site, including the lower leg and thigh, can analyze and evaluate muscle intent, facilitating applications across various research areas for robot control. The size of the sensor, the number of multiple channels, and its pattern design can be adjusted to suit the specific research application and can be tailored to the next-generation of neuroprostheses[52,53].

METHODS

Subjects

The clinical trial was exclusively conducted on individuals who met the specific inclusion and exclusion criteria and who voluntarily provided their own handwritten signature on the clinical trial consent form. The Institutional Review Board (IRB) at the Seoul National University Hospital Biomedical Research Institute further authorized the study. The study recruited three male participants who had undergone lower limb amputations. Two had undergone amputations below the knee (BK), with an average age of 39.5, and one had undergone an above-the-knee amputation. One of the participants with a BK amputation had undergone normal amputation, while the other had undergone regenerative peripheral nerve interface (RPNI) amputation within the last 3 years. All three participants used negative pressure-type sockets and silicone liners. The participant who had undergone RPNI surgery participated in the electromyography (EMG) test in a dynamic state, while the other two participants participated in the EMG test in a static state.

Numerical simulation

The stress–strain curve generated from the electrode structure was numerically calculated using COMSOL Multiphysics software. We analyzed a part of the pattern to shorten the simulation time and reduce the amount of calculation. Solid and shell models were used to analyze the proposed design, and a 5 μm polyimide film with a serpentine structure was formed on a substrate layer consisting of 70 μm PDMS and 270 μm Silbione. The proposed pattern was placed on a 5 × 5 cm square piece of skin with a thickness of 1700 μm, and Au was created as a thin 200 nm film on that. The physical properties of the materials can be found in Supplementary Table 1. For the substrate layer, we used the experimental values we measured, and for the electrode layer, we used the values stored in the COMSOL library. As boundary conditions, one side of the skin was assigned a fixed displacement, and a displacement of 0 to 45 mm was applied to the opposite side of the skin. The maximum value of the stress was calculated on the surface of the Au thin film according to the strain.

Signal recording with Intan

For the measurements, electrical signals were recorded by connecting an Intan RHD2216 and an RHD Intan Develop Board. The potential difference detected by the proposed sEMG sensor was amplified by a bioamp. It was delivered to the Develop Board through an SPI cable, a USB 2.0 cable was connected to a laptop, and the signal detected by the Intan RHX software, a viewer program, could be checked and saved. In signal processing, the low-pass and high-pass filters of the analog filter could be controlled through the analog filter in RHD2216 using the viewer program. A 60 Hz notch filter was applied to the 20 to 500 Hz bandpass range. The measured signal was analyzed through MATLAB to rectify the signal and smoothed using a moving average window of 150 ms. Finally, it was divided into maximum values and normalized. We used the following theoretical values for comparison of the proposed sEMG and commercial electrodes:

$$\mathrm{SNR} = 20 \times \log_{10} \frac{V_{\mathrm{RMS\ EMG}}}{V_{\mathrm{RMS\ Baseline\ Noise}}} \tag{1}$$

$$\mathrm{Sensitivity} = \frac{V_{\mathrm{RMS\ EMG}} - V_{\mathrm{RMS\ Baseline\ Noise}}}{F} \tag{2}$$

where $V_{\mathrm{RMS\ EMG}}$ and $V_{\mathrm{RMS\ Baseline\ Noise}}$ represent the rms values for the contraction region and baseline region, respectively. F represents the maximum measured force. We calculated the SNR and sensitivity and compared them with those of commercial electrodes.

$$\mathrm{Threshold} = \mu \times 3\sigma \tag{3}$$

$$\mathrm{Pearson's\ Coefficient} = \frac{\sum_{i=1}^{n} \left(V_{\mathrm{Com,i}} - \overline{V}_{\mathrm{Com}}\right)\left(V_{\mathrm{sEMG,i}} - \overline{V}_{\mathrm{sEMG}}\right)}{\left\{\sum_{i=1}^{n} \left(V_{\mathrm{Com,i}} - \overline{V}_{\mathrm{Com}}\right)^2 \sum_{i=1}^{n} \left(V_{\mathrm{sEMG,i}} - \overline{V}_{\mathrm{sEMG}}\right)^2\right\}^{1/2}} \tag{4}$$

where μ and σ are the mean and standard deviation of the linear envelope during the first second of rest at the beginning of each trial. 3σ was selected to clearly distinguish between the baseline noise and the muscle signal generated by contraction. V_{Com} and V_{sEMG} indicate the muscle signals obtained by the commercial electrodes and proposed electrodes, respectively. The muscle-on time and muscle-off time were calculated by applying threshold values to linear envelope muscle signals. For muscle signals obtained with the commercial and proposed sEMG electrodes, the Pearson's correlation between the muscle-on time and -off time of linear envelope signals were calculated.

$$\mathrm{Selectivity\ Ratio} = \mathrm{SNR}_{\mathrm{agonist}} / \mathrm{SNR}_{\mathrm{antagonist}} \tag{5}$$

We calculated the selectivity ratio to calculate how clearly signals could be distinguished for dorsiflexion and plantar flexion in TA and GC muscles. Here, $\mathrm{SNR}_{\mathrm{agonist}}$ is the SNR measured in the muscle that is mainly active for an action, and $\mathrm{SNR}_{\mathrm{antagonist}}$ is the SNR of the muscle signal measured in the antagonist muscle.

Mechanical characterization

Tensile measurements for the substrate layer were conducted using a universal testing machine (United Calibration, SFM-100kN, India). The equipment was clamped to an end of the 5 cm square substrate and stretched the substrate at a 20 mm min^{-1} speed. A Bending & Stretchable Machine System (SNM, Korea) was used to test the resistance change of the sEMG sensor depending on the strain. The bending machine clamped both ends of the substrate and stretched it to 65% at a rate of 1 mm/s. A resistance meter was connected to the sEMG sensor to observe the change in the resistance in real time.

Adhesion force and impedance measurement

The adhesion force of a substrate was measured through the delamination process using a universal testing machine (AIP, MultiTest 2.5-i, USA). The adhesion force of a substrate was measured through the delamination process using a universal testing machine (AIP, MultiTest 2.5-i, USA). The proposed sEMG sensor was peeled off at 90° with a speed of 10 mm min^{-1} fixed to one end. The device's attachment area measures 300 mm^2 and is ~90% detached in the peel test. The lightly polished pig skin surface and the sEMG sensor were used 10 times, and the contact impedance and force were measured between the attachment and detachment processes. An electrochemical impedance spectroscopy (HS Technologies, nStat, Korea) was used for impedance measurement, and the commercial electrode was connected to the counter electrode and the LG electrode was connected to the working electrode, and the impedance was measured for the frequency from 1 Hz to 1 kHz in a two-electrode configuration.

System setup in the static test

The proposed sEMG sensor was attached to the TA, GC, VM, and VL muscles for patients with lower leg amputation. After lightly wiping the epidermis of the target muscle area, a sensor was attached, and liners and sockets were not worn. The patient sat still and contracted the target muscle according to the instructions, and we succeeded in controlling the robot with wireless and wired systems using Intan and M40 devices (Supplementary Figs. 7 and 8).

System setup in the dynamic test

TA and GC muscles were tested for a lower leg patient who underwent RPNI surgery. After lightly wiping the epidermis of the target muscle, a sensor was attached. After combining an RHD2216 Arduino Shield with an Arduino Uno, it was connected to a Raspberry Pi 4 using a USB 2.0 AB connector to build a wireless system (Supplementary Fig. 9). An additional lithium-ion battery module was installed so that the system could be used for 4–5 h without charging. A case was formed using a 3D printer to protect the wireless system circuitry from external impacts and to mount it as a socket in Fig. 6a. We selected thresholds based on the patient's EMG signal. The identification of the EMG signal is shown in Supplementary Fig. 10. When the threshold value was exceeded, Bluetooth was used for communication, and 1 and 0 were delivered to the robotic leg.

WVTR test

The WVTR test measured how much 5 ml of water contained in a cylindrical container with a radius of 15 mm evaporated over 24 h when the container was sealed with P-PDMS. The mass in the initial state was measured, and the mass was measured again after a day. The experiment was conducted in an environment of 23° Celsius and 50% humidity.

DATA AVAILABILITY

All data generated in this study, including source data and the data used to make the figures, are available from figshare with 538 the identifier https://doi.org/10.6084/m9.figshare.24258418. Supplementary datasets are provided with this paper.

CODE AVAILABILITY

The underlying code for this study is not publicly available but may be made available to qualified researchers on reasonable request form the corresponding author.

Received: 25 May 2023; Accepted: 13 October 2023;
Published online: 25 October 2023

REFERENCES

1. Kim, D.-H. et al. Epidermal electronics. *Science* **333**, 838–843 (2011).
2. Wang, S. et al. Physiology-based stretchable electronics design method for accurate surface electromyography evaluation. *Adv. Sci.* **8**, 2004987 (2021).
3. Wang, C. et al. Stretchable, multifunctional epidermal sensor patch for surface electromyography and strain measurements. *Adv. Intell. Syst.* **3**, 2100031 (2021).
4. Chandra, S. et al. Performance evaluation of a wearable tattoo electrode suitable for high-resolution surface electromyogram recording. *IEEE Trans. Biomed. Eng.* **68**, 1389–1398 (2020).
5. Sadikoglu, F., Kavalcioglu, C. & Dagman, B. Electromyogram (EMG) signal detection, classification of EMG signals and diagnosis of neuropathy muscle disease. *Procedia Comput. Sci.* **120**, 422–429 (2017).
6. Meigal, A. Y., Rissanen, S., Zaripova, Y. R., Miroshnichenko, G. & Karjalainen, P. Nonlinear parameters of surface electromyogram for diagnostics of neuromuscular disorders and normal conditions of the human motor system. *Hum. Physiol.* **41**, 672–679 (2015).
7. Murphy, B. B. et al. A gel-free Ti3C2Tx-based electrode array for high-density, high-resolution surface electromyography. *Adv. Mater. Technol.* **5**, 2000325 (2020).
8. Driscoll, N. et al. MXene-infused bioelectronic interfaces for multiscale electrophysiology and stimulation. *Sci. Transl. Med.* **13**, eabf8629 (2021).
9. Yu, Y. et al. All-printed soft human-machine interface for robotic physicochemical sensing. *Sci. Robot.* **7**, eabn0495 (2022).
10. Zeng, X., Dong, Y. & Wang, X. Flexible electrode by hydrographic printing for surface electromyography monitoring. *Materials* **13**, 2339 (2020).
11. Huang, C.-Y. & Chiu, C.-W. Facile fabrication of a stretchable and flexible nanofiber carbon film-sensing electrode by electrospinning and its application in smart clothing for ECG and EMG monitoring. *ACS Appl. Electron. Mater.* **3**, 676–686 (2021).
12. Li, J. et al. High-performance flexible microneedle array as a low-impedance surface biopotential dry electrode for wearable electrophysiological recording and polysomnography. *Nano Micro Lett.* **14**, 132 (2022).
13. Hargrove, L. J. et al. Robotic leg control with EMG decoding in an amputee with nerve transfers. *N. Engl. J. Med.* **369**, 1237–1242 (2013).
14. Fleming, A. et al. Myoelectric control of robotic lower limb prostheses: a review of electromyography interfaces, control paradigms, challenges and future directions. *J. Neural Eng.* **18**, 041004 (2021).
15. Hussain, T. et al. Intent based recognition of walking and ramp activities for amputee using sEMG based lower limb prostheses. *Biocybern. Biomed. Eng.* **40**, 1110–1123 (2020).
16. Salminger, S. et al. Long-term implant of intramuscular sensors and nerve transfers for wireless control of robotic arms in above-elbow amputees. *Sci. Robot.* **4**, eaaw6306 (2019).
17. Srinivasan, S. et al. On prosthetic control: a regenerative agonist-antagonist myoneural interface. *Sci. Robot.* **2**, eaan2971 (2017).
18. Klute, G. K., Glaister, B. C. & Berge, J. S. Prosthetic liners for lower limb amputees: a review of the literature. *Prosthet. Orthot. Int.* **34**, 146–153 (2010).
19. Huang, S. & Ferris, D. P. Muscle activation patterns during walking from transtibial amputees recorded within the residual limb-prosthetic interface. *J. Neuroeng. Rehabil.* **9**, 1–16 (2012).
20. Clites, T. R. et al. Proprioception from a neurally controlled lower-extremity prosthesis. *Sci. Transl. Med.* **10**, eaap8373 (2018).
21. Hefferman, G. M., Zhang, F., Nunnery, M. J. & Huang, H. Integration of surface electromyographic sensors with the transfemoral amputee socket: a comparison of four differing configurations. *Prosthet. Orthot. Int.* **39**, 166–173 (2015).

22. Yeon, S. H. et al. Flexible dry electrodes for EMG acquisition within lower extremity prosthetic sockets. *2020 8th IEEE RAS/EMBS International Conference for Biomedical Robotics and Biomechatronics (BioRob)* 1088–1095 (IEEE, 2020).
23. Bonnefoy-Mazure, A. & Armand, S. Normal gait. *Orthop. Manag. Child. Cereb. Palsy* **40**, 567 (2015).
24. Cho, S. et al. Wireless, AI-enabled wearable thermal comfort sensor for energy-efficient, human-in-the-loop control of indoor temperature. *Biosens. Bioelectron.* **223**, 115018 (2023).
25. Chao, S. et al. Synthesis and characterization of tigecycline-loaded sericin/poly (vinyl alcohol) composite fibers via electrospinning as antibacterial wound dressings. *J. Drug Deliv. Sci. Technol.* **44**, 440–447 (2018).
26. Yoon, S., Seok, M., Kim, M. & Cho, Y.-H. Wearable porous PDMS layer of high moisture permeability for skin trouble reduction. *Sci. Rep.* **11**, 938 (2021).
27. Lamke, L.-O., Nilsson, G. A. & Reithner, H. The evaporative water loss from burns and the water-vapour permeability of grafts and artificial membranes used in the treatment of burns. *Burns* **3**, 159–165 (1977).
28. Srivastava, C. M., Purwar, R. & Gupta, A. P. Enhanced potential of biomimetic, silver nanoparticles functionalized Antheraea mylitta (tasar) silk fibroin nanofibrous mats for skin tissue engineering. *Int. J. Biol. Macromol.* **130**, 437–453 (2019).
29. Krysiak, Z. J., Knapczyk-Korczak, J., Maniak, G. & Stachewicz, U. Moisturizing effect of skin patches with hydrophobic and hydrophilic electrospun fibers for atopic dermatitis. *Colloids Surf. B Biointerfaces* **199**, 111554 (2021).
30. Tantua, A. T., Geertzen, J. H., van den Dungen, J. J., Breek, J.-K. C. & Dijkstra, P. U. Reduction of residual limb volume in people with transtibial amputation. *J. Rehabil. Res. Dev.* **51**, 1119–1126 (2014).
31. Su, H., Kim, T.-H., Moeinnia, H. & Kim, W. S. A 3-D-printed portable EMG wristband for the quantitative detection of finger motion. *IEEE Sens. J.* **23**, 7895–7901 (2023).
32. Dong, W., Zhu, C., Hu, W., Xiao, L. & Huang, Y. A. Stretchable human-machine interface based on skin-conformal sEMG electrodes with self-similar geometry. *J. Semicond.* **39**, 014001 (2018).
33. Gong, Q., Jiang, X., Liu, Y., Yu, M. & Hu, Y. A flexible wireless sEMG system for wearable muscle strength and fatigue monitoring in real time. *Adv. Electron. Mater.* **9**, 2200916 (2023).
34. Stegeman, D. & Hermens, H. Standards for surface electromyography: the European project Surface EMG for non-invasive assessment of muscles (SENIAM). *Enschede Roessingh Res. Dev.* **10**, 8–12 (2007).
35. Nie, S., Cai, M., Wang, C. & Song, J. Fatigue life prediction of serpentine interconnects on soft elastomers for stretchable electronics. *J. Appl. Mech.* **87**, 011011 (2020).
36. Kalra, A., Lowe, A. & Al-Jumaily, A. Mechanical behaviour of skin: a review. *J. Mater. Sci. Eng.* **5**, 1000254 (2016).
37. Posada-Quintero, H. F., Rood, R. T., Burnham, K., Pennace, J. & Chon, K. H. Assessment of carbon/salt/adhesive electrodes for surface electromyography measurements. *IEEE J. Transl. Eng. Health Med.* **4**, 1–9 (2016).
38. Nussinovitch, A., Gal, A., Padula, C. & Santi, P. Physical characterization of a new skin bioadhesive film. *AAPS Pharmscitech* **9**, 458–463 (2008).
39. Liu, L. et al. Silicone-based adhesives for long-term skin application: cleaning protocols and their effect on peel strength. *Biomed. Phys. Eng. Express* **4**, 015004 (2017).
40. Fylstra, B. L., Dai, C., Hu, X. & Huang, H. H. Characterizing residual muscle properties in lower limb amputees using high density EMG decomposition: a pilot study. *2018 40th Annual International Conference of the IEEE Engineering in Medicine and Biology Society (EMBC)* 5974–5977 (IEEE, 2018).
41. Campbell, E. et al. Differences in EMG feature space between able-bodied and amputee subjects for myoelectric control. *2019 9th International IEEE/EMBS Conference on Neural Engineering (NER)* 33–36 (IEEE, 2019).
42. Isakov, E., Keren, O. & Benjuya, N. Trans-tibial amputee gait: time-distance parameters and EMG activity. *Prosthet. Orthot. Int.* **24**, 216–220 (2000).
43. Tintle, L. S. M., Keeling, C. J. J., Shawen, L. S. B., Forsberg, L. J. A. & Potter, M. B. K. Traumatic and trauma-related amputations: part I: general principles and lower-extremity amputations. *JBJS* **92**, 2852–2868 (2010).
44. Liu, Y., Pharr, M. & Salvatore, G. A. Lab-on-skin: a review of flexible and stretchable electronics for wearable health monitoring. *ACS Nano* **11**, 9614–9635 (2017).
45. Xu, Y. et al. Pencil–paper on-skin electronics. *Proc. Natl Acad. Sci.* **117**, 18292–18301 (2020).
46. Kumar, P. K., Charan, M. & Kanagaraj, S. Trends and challenges in lower limb prosthesis. *IEEE Potentials* **36**, 19–23 (2017).
47. Kwak, J. W. et al. Wireless sensors for continuous, multimodal measurements at the skin interface with lower limb prostheses. *Sci. Transl. Med.* **12**, eabc4327 (2020).
48. Roll, R., Kavounoudias, A. & Roll, J.-P. Cutaneous afferents from human plantar sole contribute to body posture awareness. *Neuroreport* **13**, 1957–1961 (2002).
49. Pearson, K. Role of sensory feedback in the control of stance duration in walking cats. *Brain Res. Rev.* **57**, 222–227 (2008).
50. Rossignol, S., Dubuc, R. & Gossard, J.-P. Dynamic sensorimotor interactions in locomotion. *Physiol. Rev.* **86**, 89–154 (2006).
51. Valle, G. et al. Mechanisms of neuro-robotic prosthesis operation in leg amputees. *Sci. Adv.* **7**, eabd8354 (2021).
52. Lan, N. et al. Next-generation prosthetic hand: from biomimetic to biorealistic. *Research* **2021**, 4675326 (2021).
53. Sharma, T., Sharma, K. P. & Veer, K. Evaluation of electromyogram signals in the control of prosthetic limb: a review. *Curr. Signal Transduct. Ther.* **17**, 3–11 (2022).

ACKNOWLEDGEMENTS

This research was supported by a Korea Medical Device Development Fund grant funded by the Korea government (the Ministry of Science and ICT, the Ministry of Trade, Industry and Energy, the Ministry of Health & Welfare, the Ministry of Food and Drug Safety) (Project Number: 1711135031, KMDF_PR_20200901_0158-05).

AUTHOR CONTRIBUTIONS

S.L. supervised the research. J.P. designed and carried out experiments. J.J. improved the substrate layer. N.P., Y.C., Ho.K., and S.K. helped with the robotic control. S.M. and B.K. provided robot legs. M.K., J.H., Hy.K., H.P.S., C.J.P., and J.P. recruited clinical patients and helped with clinical trials. K.J., J.Y., and J.H. helps with experiments and simulations evaluating the mechanical and electrical properties of the proposed sEMG.

COMPETING INTERESTS

The authors declare no competing interests.

ADDITIONAL INFORMATION

Supplementary information The online version contains supplementary material available at https://doi.org/10.1038/s41528-023-00282-z.

Correspondence and requests for materials should be addressed to Sanghoon Lee.

Reprints and permission information is available at http://www.nature.com/reprints

Publisher's note Springer Nature remains neutral with regard to jurisdictional claims in published maps and institutional affiliations.